Showcasing research from Professor Santra's laboratory, NanoScience Technology Center, University of Central Florida, FL, USA.

Mechanistic insights into the synergistic antimicrobial activity of nanodelivered sodium polysulfide as a sustainable strategy to combat *Xanthomonas* pathogens

Interdisciplinary research from the University of Central Florida delving into the mode of action of nano-magnesium hydroxide conjugated with sodium polysulfide as a sustainable crop protection tool to combat *Xanthomonas* pathogens. This comprehensive investigation correlates material physicochemical properties and computational models with the formulation's antimicrobial and peroxide-inducing activity. Overall, the outcomes demonstrate that nano and conventional agrochemicals can be used in combination to obtain even more favourable outcomes.

Image reproduced by permission of Jorge Pereira from *Nanoscale*, 2025, **17**, 22174.

As featured in:

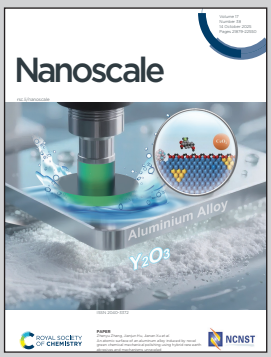

See Jorge Pereira, Swadeshmukul Santra *et al.*, *Nanoscale*, 2025, **17**, 22174.

ROYAL SOCIETY OF CHEMISTRY

rsc.li/nanoscale

Registered charity number: 207890

Nanoscale

ROYAL SOCIETY OF CHEMISTRY

PAPER

View Article Online
View Journal | View Issue

Cite this: *Nanoscale*, 2025, **17**, 22174

Mechanistic insights into the synergistic antimicrobial activity of nanodelivered sodium polysulfide as a sustainable strategy to combat *Xanthomonas* pathogens

Jorge Pereira, *[a,b] Edwin Davidson, [a,b] Melissa M. Deinys,[b,c] Allison Lloyd,[b] Preeti Maiti,[a,b] Javier Rivera-Huertas,[b,c] Atiya Banerjee,[a] Shengli Zou,[a] Bradley Demosthene,[b] Laurene Tetard [b,d] and Swadeshmukul Santra *[a,b,c]

Nanopesticides offer a promising avenue for crop management by enhancing efficacy over their conventional counterparts. Advances in managing surface-restricted plant pathogens have been reported using magnesium-based nanomaterials, but their role as delivery systems for conventional pesticides remains unexplored. This study introduces Nano-Magnesium Hydroxide (MgSol) as a delivery platform for Sodium Polysulfide (NaPs), elucidates the physicochemical interactions between the treatments, determines the ramifications of the changes on their antimicrobial mode of action, and evaluates the plant's response. A comprehensive investigation using theoretical and experimental approaches provides insights into the adsorption of polysulfide ions onto $Mg(OH)_2$ surfaces, leading to particle agglomeration and enhanced polysulfide stability. Temporal monitoring demonstrates that nanodelivered NaPs remain chemically active 12 times longer than the conventional counterpart. Antimicrobial assays confirm that nanodelivered NaPs possesses synergistic bactericidal activity, achieving an 8-fold greater potency than its components. Mechanistic studies unveil that nanodelivered NaPs drives intracellular peroxidation, leading to membrane disruption. Lastly, conditions for plant and seed biocompatibility are identified, with foliar residue studies showing an improvement in Mg deposition. Altogether, these findings showcase the potential of nano-enabled agrochemical delivery *via* inorganic nanoparticles to sustainably mitigate crop loss, supporting food security amidst rising global demands.

Received 21st July 2025,
Accepted 28th August 2025

DOI: 10.1039/d5nr03087k

rsc.li/nanoscale

Introduction

Phytopathogenic bacteria, responsible for worldwide losses exceeding one billion dollars each year, represent a significant threat to global food safety.[1] The *Xanthomonas* genus is particularly virulent and severely impacts a wide range of crops.[2,3] Pathogenic strains from this genus are known to cause disease in tomatoes, peppers, legumes, and leafy greens, among many other crops.[4–6] These infections not only reduce crops' productivity but can also affect the fruit and diminish marketable yield.[7,8] In order to meet the estimated food demand by 2050, it is necessary to increase crop production significantly[9–11] while minimizing crop losses due to pathogen infections.[12]

Xanthomonas often infect leaf tissues through the stomata, hydathodes, or other openings, and then multiply in the mesophyll tissues causing necrotic spots.[2] Chemical disease management of *Xanthomonas* pathogens includes copper–hydroxide biocides,[13,14] dithiocarbamate fungicides (*i.e.*, mancozeb)[15,16] and antibiotics, such as oxytetracycline.[17] Even though these chemicals are applied regularly, disease severity can still be high when conditions are favorable for the pathogens.[18–20] Nanomaterials have shown some promise to improve crop protection.[21] A recent analysis estimated that nanopesticides can provide a 19% efficacy boost in field trials compared to their conventional counterparts,[22] together with better biocompatibility, lower leaching, and better retention of activity. While the potential of nanotechnology-based strategies has been established, producing more effective crop protection tools that are also biocompatible and environmentally friendly is critical.

Magnesium oxide and hydroxide nanoparticles have garnered a lot of attention due to their antimicrobial properties

[a]*Department of Chemistry, University of Central Florida, 4111 Libra Drive, Orlando, FL 32816, USA. E-mail: jorge.pereira@ucf.edu, ssantra@ucf.edu*
[b]*NanoScience Technology Center, University of Central Florida, 12424 Research Parkway, Orlando, FL 32826, USA*
[c]*Burnett School of Biomedical Sciences, University of Central Florida, 4364 Scorpius Street, Orlando, FL 32816, USA*
[d]*Department of Physics, University of Central Florida, Orlando, FL, 32826, USA*

and lower negative environmental impact, when compared to transition metal-based nanomaterials.[23–26] Magnesium oxide nanoparticles have previously outperformed commercial products in reducing the severity of bacterial spot of tomatoes in the greenhouse, and in field conditions.[27–30] Recently, magnesium-copper hydroxide hybrid nanomaterials significantly reduced the severity of bacterial spot of tomato in field trials against copper tolerant bacterial strains.[31] Nevertheless, copper-based pesticides have been used for over a century, which has led to copper accumulation in topsoil, among other environmental issues.[32] Therefore, it is important to create alternate strategies to replace copper-based pesticides.

Using sulfur to improve performance of magnesium-based nanopesticides provides an alternative towards sustainable crop protection. As sulfur is an essential secondary macronutrient for plants,[33] it does not pose any major ecological threat, and as such, is widely used in agriculture.[34,35]

Previous works studied combinations of inorganic pesticides focused on cations also playing the role of micronutrients in plants such as Cu^{2+}, Zn^{2+}, and Fe^{3+}.[36,37] Toxicity and poor abundance constitute challenges in their implementation. When searching for alternative treatments, considering safety, economic viability, efficacy, and plant compatibility is essential.[38]

Polysulfide formulations, such as lime sulfur, are approved for agricultural use. They provide higher potency against foliar pathogens than elemental sulfur.[39,40] However, polysulfide ions undergo two main degradation reactions under ambient conditions. The primary reaction involves polysulfide oxidation:[41]

$$S_x^{2-} + 3/2O_2 \rightarrow S_2O_3^{2-} + (X-2)/8\ S_8 \quad (1)$$

Followed by their disproportionation reaction to sulfur and sulfide:[42,43]

$$S_x^{2-} \rightleftharpoons S^{2-} + (X-1)/8\ S_8 \quad (2)$$

in which $2 \leq X \leq 8$. These reactions quickly reduce the effective concentration of polysulfide ions, limiting their antimicrobial capacity. Therefore, it is imperative to improve the stability and delivery of polysulfide ions to harness their biocidal potential.

Here we report the design and evaluation of a magnesium–sulfur nanoformulation (MgSuN), prepared by using magnesium hydroxide nanoparticles (MgSol) to deliver sodium polysulfide (NaPs). To understand the first nano-enabled delivery of polysulfide pesticide using magnesium hydroxide nanoparticles, the interactions between NaPs and MgSol are studied, as well as the physicochemical changes the formulation undergoes over time. Radical scavenging assays provide insight into the effect of MgSol on the chemical properties of NaPs as a function of time. The synergistic antimicrobial properties and mode of action of MgSuN are evaluated through multiple assays (*e.g.* checkboard, MBC, DNA leakage, among others). Furthermore, the plant interactions with MgSuN are assessed to determine the formulation's safety and biocompatibility based on different concentration ratios, using *Capsicum annuum* and *Solanum lycopersicum* plants.

Materials and methods

Material synthesis

The magnesium hydroxide nanoformulation (MgSol) was synthesized using a previously published protocol.[24] Briefly, 21.1 g of magnesium nitrate hexahydrate (Thermo Fisher Scientific, Waltham, MA) and 12.1 g trisodium citrate dihydrate (Thermo Fisher Scientific, Waltham, MA) were dissolved in 60 mL of deionized water (DI) under magnetic stirring. After complete dissolution, an aqueous 5.0 M sodium hydroxide solution was added dropwise into the magnesium solution until the mixture reached a pH of 10.2. Finally, the suspension was left to stir for 24 hours before adjusting the volume with DI water to obtain a final concentration of 20 000 mg L^{-1} (ppm) of Mg.

Sodium polysulfide (NaPs) was prepared by the alkaline hydrolysis of elemental sulfur. First, 14.3 g of elemental sulfur (Thermo Fisher Scientific, Waltham, MA) were suspended in 75.0 mL of aqueous 5.0 M sodium hydroxide solution. Then, this suspension was heated to approximately 98 °C, while stirring until the elemental sulfur fully dissolved. The resulting solution exhibited a deep orange color. The concentration was adjusted to 143 000 mg L^{-1} (ppm) of S.

The MgSol and NaPs formulations were combined at low concentrations (800–200 ppm) for some of the experiments. The combinations resulted in a nanoparticle suspension that contained Mg and S, which is abbreviated as MgSuN hereafter.

Checkerboard assay

The antibacterial interactions of MgSol and NaPs on *Xanthomonas alfalfae* subsp. *citrumelonis* (*Xac*; ATCC 49120), wildtype *Xanthomonas perforans* (91–118; *Xp*),[44] and *Pseudomonas syringae* (*Ps;* ATCC 19310) were assessed using a checkerboard assay.[45,46] MgSol was serially diluted vertically in a sterile 96 well plate and NaPs was serially diluted horizontally in the same well plate. The treatment concentrations were adjusted to cover a range from 512 to 8 ppm of Mg for MgSol and 512 to 0.5 ppm of S for NaPs.

Afterwards, a bacterial suspension was adjusted to $\sim 1 \times 10^6$ CFU mL^{-1} by first adjusting the optical density at 600 nm (OD600) to 0.1 and then diluting the suspension a hundredfold in nutrient broth. Subsequently, the bacteria were added to each well to achieve a final concentration of $\sim 5 \times 10^5$ CFU mL^{-1}. The inoculated plates were set to incubate at 28 °C in an orbital shaker rotating at 150 rpm. As an indirect measurement for bacterial growth, the OD600 was measured after 48 hours using an Infinite M200 Pro (Tecan, Männedorf, Switzerland). The minimum inhibitory concentration (MIC) was defined as the lowest concentration of each series that resulted in an average OD600 lower than 0.1. All experiments were carried out in triplicates ($n = 3$).

Next, the bactericidal activity of the treatments was evaluated by inoculating a 96 well plate containing 50 μL of nutrient agar in each well, with 25 μL of treated bacterial suspensions that resulted from the checkerboard assay. The minimum bactericidal concentration (MBC) was determined as the statistical

mode of the lowest concentration in a series that prevented bacterial colonies formation after 48 hours of incubation.[47]

The Fractional Inhibitory Concentrations (FIC) was calculated based on the checkerboard results using the following equation:

$$\mathrm{FIC} = \frac{[\mathrm{NaPs}]}{\mathrm{MIC}_{\mathrm{NaPs}}} + \frac{[\mathrm{MgSol}]}{\mathrm{MIC}_{\mathrm{MgSol}}}$$

where [NaPs] and [MgSol] are the concentrations of the antimicrobials in a specific well, $\mathrm{MIC}_{\mathrm{NaPs}}$ and $\mathrm{MIC}_{\mathrm{MgSol}}$ are the MIC of the respective antimicrobials. The interaction between NaPs and MgSol were categorized using the FIC values: values over 4 were deemed as antagonistic, values between 4–0.5 were regarded as additive and values under 0.5 were considered to be synergistic. The Fractional Bactericidal Concentrations (FBC) were also calculated using the same equation by replacing the MIC with the MBC results. The resulting FBC values were subjected to the same criteria as the FIC to categorize the bactericidal interaction of MgSuN.

DNA leakage assay

Bacterial cells were cultured in nutrient broth for 24 hours in an orbital shaker incubator (Inova 4000, New Brunswick Scientific) at 150 rpm and 28 °C. After incubation, the bacterial stock solution was centrifuged at 5000 rpm for 10 minutes to pellet the cells. The pellet was then resuspended in a sterile 10 mM $MgSO_4$ solution and adjusted to an OD600 of 0.1. Subsequently, the suspension was diluted to obtain a final cell density of approximately 1×10^6 CFU mL^{-1}. Afterwards, the bacteria were treated with MgSuN (64 ppm Mg/2 ppm S), NaPs (2 ppm S), MgSol (64 ppm Mg), or left untreated, and incubated at 28 °C on an orbital shaker at 150 rpm for 4 hours. Following this period, the bacteria were centrifuged at 10 000 rpm for 10 minutes and the supernatant was collected to measure the absorbance at 260 nm using a Synergy H1 Microplate Reader (Agilent, Santa Clara, CA) given that DNA absorbs at this wavelength. All experiments were conducted in triplicates ($n = 3$).

Intracellular reactive oxygen species (ROS) quantification

To evaluate oxidative stress induced by the treatments, intracellular ROS was measured using 2′,7′-dichlorofluorescein diacetate (DCFH-DA; Thermo Fisher Scientific, Waltham, MA), following established protocols.[25] For this, bacterial pellets obtained following the DNA leakage assay were resuspended in 2 mL of 10 mM $MgSO_4$ and DCFH-DA was added to achieve a final concentration of 10 μM in solution. Subsequently, the samples were incubated in the dark for 30 minutes to allow the dye to react with the ROS. Then the stained samples were centrifuged (10 000 rpm for 10 min) and resuspended in a 10 mM $MgSO_4$ solution to eliminate residual dye. Finally, the bacterial suspensions were resuspended in 0.8 mL of the $MgSO_4$ solution and aliquoted into a 96-well microplate. To ensure homogeneity, the plate was agitated for 10 seconds before analysis. The fluorescence intensity at 520 nm (excitation $\lambda = 485$ nm) was measured using a plate reader.

The specific ROS species were identified using a variation of a previously reported methodology.[48] First, intracellular hydrogen peroxide (H_2O_2) levels were investigated using a Fluorometric Hydrogen Peroxide Assay Kit (Sigma–Aldrich, St Louis, MO), following the manufacturer's instructions. For this, the bacterial suspensions were treated and purified, similarly to the DNA leakage protocol, and then incubated with the assay working solution containing a red peroxidase substrate and horseradish peroxidase. This resulted in a fluorescent signal dependent on the oxidation of the substrate caused by H_2O_2. After a 30-minute incubation in the dark, the fluorescence at 590 nm (excitation $\lambda = 540$ nm) was measured using a plate reader.

Intracellular hydroxyl radical levels were also assessed, using hydroxyphenyl fluorescein (HPF; MedChemExpress, Monmouth Junction, NJ). In this case, the treated bacterial suspensions were centrifuged at 5000 rpm for 10 minutes, and the resulting pellets were washed once with 10 mM $MgSO_4$. Following this, the pellets were resuspended in 1.0 mL of 10 mM $MgSO_4$ containing 10 μM of the HPF. Finally, the samples were incubated in the dark at room temperature for 15 minutes and transferred to a 96-well microplate, where the fluorescence was measured (emission $\lambda = 520$ nm and excitation $\lambda = 490$ nm).

All fluorescent readings were performed using a Synergy H1 Microplate Reader (Agilent, Santa Clara, CA). Furthermore, the experiments included untreated bacterial suspensions and treatment-dye solutions as blanks, and each sample was analyzed in triplicate ($n = 3$).

Raman and UV-Visible spectroscopy

The content in polysulfide of the solutions was assessed using Raman and UV-Visible spectroscopies. Raman spectra were collected using a confocal Raman Microscope (Horiba LabRAM HR Evolution Nano, Japan) equipped with a SIN-EM FIUV detector and a 532 nm excitation laser. 10.0 μL of the sodium polysulfide solution was deposited on a glass slide. The excitation laser was focused in the droplet volume using a 10× objective. A pinhole aperture of 100 μm was used for the confocal microscope. Raman spectra (20–675 cm^{-1}) were acquired using a 1800 m per gr grating, an acquisition time of 15 s and 5 accumulations.

UV-Visible spectra were acquired with a Synergy H1 Microplate reader (Agilent, Santa Clara, CA). Initially, the samples were serially diluted by half, using DI water, in a 96-well plate. UV-Visible spectra were collected from 230–700 nm, using a step size of 2 nm.

Scanning electron microscopy and energy dispersive spectroscopy

The changes in morphology MgSuN undergoes over the course of 24 hours under magnetic stirring were studied using Scanning electron microscopy (SEM). Initially, MgSol and NaPs were diluted to 800 ppm of Mg and 400 ppm of S, respectively, using DI under magnetic stirring. Then samples were collected 24 hours after the dilutions. The samples were

centrifuged at 12 000 rpm for 10 minutes and the resulting pellet was resuspended in DI. The separation and resuspension steps were repeated two more times before drop-casting the suspension on a silicon wafer. The SEM images of the dried residue were obtained using the Inlens detector of a Zeiss Nvision 40 (Zeiss, Oberkochen, Germany). The experiment was also performed utilizing NaPs, to understand the effect of MgSol in the morphology of the resulting particulate after 24 hours of stirring. EDS spectra were collected using a Hitachi TM 3000 (Hitachi, Tokyo, Japan) from purified MgSuN samples obtained after 0, 2, 4, 8, and 24 hours of stirring.

Fourier transformed infrared spectroscopy and X-ray diffraction

Changes in crystallinity that the treatments undergo over 24 hours were studied using Fourier Transformed Infrared Spectroscopy (FTIR) and X-ray diffraction (XRD). The formulations were diluted with DI to obtain a final concentration of 800 ppm of Mg for MgSol, 800 ppm of S for NaPs or 600 ppm Mg, and 200 ppm S for MgSuN. After stirring for 24 hours, the particles were separated and purified by centrifuging the suspensions at 12 000 rpm for 10 minutes and washing the pellet with DI three times. After that, the suspensions were frozen and lyophilized (FreezeZone, Labconco, Kansas City, MO). The powder was analyzed by XRD using a PANalytical Empyrean XRD (Malvern Panalytical, Malvern, UK) set at 45 kV/20 mA, using a scan speed of 0.06° s^{-1}, and a step size of 0.05°. The infrared spectra were collected with a Spirit spectrometer (Shimadzu, Kyoto, Japan) equipped with a single-reflection attenuated total reflectance attachment (QATR-S), averaging 40 scans at a resolution of 1.42 cm^{-1}.

Computational models

The polysulfide ion adsorption onto the surface of the $Mg(OH)_2$ present in MgSol was analyzed using computational models. An optimized bulk $Mg(OH)_2$ structure was used to generate surface models with appropriate thickness for estimating both bulk and surface behaviour. Sodium polysulfides (Na_2S_x) were considered to describe the polysulfide species for adsorbate models as it is well established that conformationally, polysulfides can aggregate in both ordered and disordered forms.[49] The number of sulfur atoms involved ranged from 1 to 8.

Surface adsorbate models were built in VASP[50–54] and subjected to DFT calculations employing the PBE exchange–correlation functional[55] to describe the non-classical effects. However, an implicit model, laid out in VASPsol, was utilized to describe the solvent effects of the aqueous synthesis environment.[56,57] Additional details of the computational protocol are provided in the SI.

Radical scavenging activity

To determine the effect of MgSol on the reactivity of polysulfide ions, a radical scavenging assessment was performed using a 2,2-diphenyl-1-picrylhydrazyl (DPPH, Fisher Scientific, Pittsburgh, PA) assay with some modifications.[47,58] Firstly, MgSuN samples were prepared at different concentrations of Mg : S (0 : 60, 20 : 60, 60 : 60, and 180 : 60 ppm) and stirred for up to 24 hours to evaluate how different concentration ratios affected polysulfide degradation. Aliquots were collected at 0, 2, 8, 16, and 24 hours for the radical scavenging activity assessment. Then, absorbance spectra were recorded from 300 to 700 nm using a Synergy H1 Microplate Reader (Agilent, Santa Clara, CA) upon mixing 10 μL of the DPPH stock solution (0.25 mg mL^{-1}) with 190 μL aliquot of the samples in a well plate.

Assessment of phytotoxicity, rainfastness and chemical residue

Capsicum annuum (Sweet Bell Pepper variety) and *Solanum lycopersicum* (Better Boy variety) were sourced locally (Bonnie Plants, Union Springs, AL). The plants' foliage was thoroughly washed with DI and the plants were placed in a growth chamber (Panasonic, Japan) set at 25 °C, 60% relative humidity and 18 h/6 h day-night cycle, for 3 days. After the acclimatization period, the plants were sprayed with 25 mL of the formulations, left to air dry and reintroduced into the growth chamber. The phytotoxicity, rainfastness, and chemical residues on the leaves were evaluated 72 hours after the foliar application. The phytotoxicity was evaluated according to a severity scale with four levels (unaffected, minimal, moderate, and severe), based on the incidence of necrotic tissues and leaf burn.[59] The leaves were categorized according to the scale and the percentage of leaves affected was calculated. Three plants (n = 3) were utilized for the phytotoxicity evaluation. Additionally, tissue samples were collected and the chemical residue on the surface of leaves was imaged using EDS on a Hitachi TM 3000 SEM (Hitachi, Tokyo, Japan) operated at 15 kV. The rainfastness was evaluated according to a previously published protocol.[60] Leaf samples of each treatment (n = 4) were collected and subjected to 3 consecutive DI immersions to simulate rainfall events. Lastly, the samples were immersed in 0.1 M HCl to remove all the material that was still adhered to the cuticle. All immersions were performed in conical centrifuge tubes, using 40 mL of volume for 30 seconds with tumbling, to ensure the leaf was completely immersed. The concentration of Mg^{2+} in the washes was quantified through Atomic Absorption Spectroscopy (AAS) with an AAnalyst 400 Spectrometer (PerkinElmer, Waltham, MA) utilizing a calibration curve ranging from 2–0.125 μg Mg mL^{-1} prepared using a 1 mg Mg mL^{-1} standard solution (Thermo Fisher Scientific, Waltham, MA).

Seed priming studies

Seed priming experiments were performed to understand the effect of the formulations on germination. For this, 30 sweet bell pepper seeds (Sow Right Seeds, Greenwood, MO) were submerged in 45 mL of different treatments for 24 hours. Afterwards, 10 seeds for each treatment were sown individually in 4-inch pots filled with commercial potting mix (The Scotts Miracle-Gro Company, Marysville, OH) and placed in a greenhouse. MgSuN, MgSol, and NaPs treatments were applied at

64 ppm Mg/32 ppm S, 32 ppm Mg/16 ppm S, and 16 ppm Mg/8 ppm S, respectively. Magnesium sulfate heptahydrate (Thermo Fisher Scientific, Waltham, MA) was used as a control. To assess if the treatments slow down seed germination, the number of seedlings emerging from the soil was recorded daily for a period of 30 days. Each treatment was evaluated in duplicates.

Statistical analysis

The data collected from the phytotoxicity and rainfastness experiments was analyzed using a two-way ANOVA. A Tukey *post hoc* test was conducted utilizing GraphPad Prism 10.2.2 (GraphPad Software Inc., Boston, MA), setting multiple means comparisons across independent variables, using a p-value of 0.05.

Results and discussion

Material characterization

The $Mg(OH)_2$ coprecipitation methodology afforded a milky suspension capable of light diffraction upon dilution. The solution obtained from NaPs synthesis exhibited a deep orange solution, studied using Raman and UV-Visible spectroscopies (Fig. S1). Raman peaks at 486, 448, 249, and 199 cm^{-1}, are attributed to the presence of S_3^{2-}, S_4^{2-}, and S_5^{2} polysulfide species.[61,62] UV-Vis absorbance at 394, 367, and 303 nm also confirmed the presence of polysulfide ions, namely S_3^{2-}, S_4^{2-}, and S_5^{2-} in the solution.[63] The magnesium–sulfur nanoformulation (MgSuN) was designed to harness the superior surface to volume ratio of nano $Mg(OH)_2$ contained in MgSol, to adsorb and deliver polysulfide ions while retaining its antimicrobial activity. The nanoformulation was prepared with different ratios to elucidate the mechanistic behavior between the interactions of MgSol and NaPs to identify conditions for synergistic antimicrobial efficacy. When maintaining the S content at 800 ppm and varying the Mg content from 0 to 800 ppm, different stability levels were observed for the suspensions after 24 hours of mixing (Fig. S2). The effect of NaPs on the hydrodynamic size of MgSol was assessed with DLS (Fig. 1A). The particles in MgSol exhibited an average hydrodynamic diameter of 190 nm, while a much broader distribution centered at 342 nm was observed for the MgSuN particles. The zeta potential of formulations was also analysed (Table S1), but only from −25 mV to −23.8 mV upon addition of NaPs. This slight reduction might suggest the presence of polysulfide ions around the particle, which possess less charge density compared to citrate ions.

After purification, the composition of the nanoparticles was assessed by FTIR spectroscopy (Fig. 1B). The spectrum of the MgSol particles exhibited an asymmetric peak at 1566 cm^{-1} attributed to carboxylate, and a peak at 1390 cm^{-1} attributed to the citrate capping agent.[30] The NaPs spectrum displayed peaks at 1114 cm^{-1} and 998 cm^{-1} corresponding to S–O.[64,65] The MgSuN spectra exhibited peaks at 1577 cm^{-1} and 1397 cm^{-1}, corresponding to carbonyl and carboxylate, and peaks at 1118 cm^{-1} and 1004 cm^{-1} attributed to S–O, suggesting that NaPs and the products of its oxidation adhere to the surface of the $Mg(OH)_2$ nanoparticles from MgSol. Moreover, the shift in the carbonyl peaks and the change in their relative intensities indicate a change in the chemical environment surrounding the $Mg(OH)_2$ particles in presence of NaPs. To corroborate the adsorption of NaPs onto the particles, aliquots of MgSuN were purified after stirring for different periods of time and analyzed using EDS (Fig. 1C). The resulting spectra indicate that the adsorption process requires time for the ions to interact with the particles, as MgSuN without stirring did not present the characteristic signal for sulfur at 2.31 keV,[66] but samples obtained after 2 hours of stirring exhibited a sulfur signal. The decrease in intensity observed for samples with longer stirring time could be attributed to the oxidation of the polysulfide ions into highly soluble sulfur oxyanions and sulfides that desorb from the particles during the purification process. Additionally, UV-Vis of the purified samples (Fig. S3) demonstrated increased absorption at 370 and 395 nm, compared to MgSol, which would indicate the adsorption of S_4^{2-} and S_5^{2-} onto the particles.

SEM images of MgSuN and NaPs, acquired after 24 hours of mixing (Fig. 1D & E), revealed aggregates of nanoparticles (40–300 nm) with irregular morphologies for MgSuN (Fig. 1D) and an amorphous precipitated in NaPs (Fig. 1E). This is in agreement with visible changes the solution of MgSuN undergoes after 24 hours of stirring (Fig. S2).

The crystallinity of the materials was analyzed by XRD (Fig. 1G & H). The diffractogram from the purified degradation product of NaPs (Fig. 1H) exhibited features similar to those observed for sulfur crystals (α-sulfur crystal pattern),[67] suggesting that NaPs decomposes into sulfur crystals, as described in reaction (1) and (2). This is in agreement with NaPs agglomeration and formation of large-sized precipitate when stirred for 24 hours (Fig. S2), given that α-sulfur is insoluble in water. The XRD pattern of purified MgSuN was found to be similar to that of MgSol (Brucite).[24,30] However, the MgSuN reflections at 37.8 and 59.0 degrees exhibited higher intensity than that of MgSol (Fig. 1G). Based on literature, these reflections are assigned to the (101) and (110) crystal lattices. It has been shown that ions can affect the relative intensity of (001), (101), and (110) through adsorption, dissolution or co-precipitation processes.[68–70] Additionally, the absence of diffraction peaks from α-sulfur in MgSuN's diffractogram, suggests that in the presence of MgSol, NaPs does not degrade into α-sulfur.

Many sulfur compounds, such as sulfides, are byproducts from industrial processes and must be separated from effluxes. Double-layered hydroxides and magnesium-based nanomaterials have been utilized to remove sulfur compounds from waste gases through adsorption.[71,72] These observations align with the present results, suggesting NaPs adsorption to the surface of MgSol during the mixing process. Considering all these findings, the proposed mechanism of nano-mediated stabilization of polysulfide ions with $Mg(OH)_2$ nanoparticle is

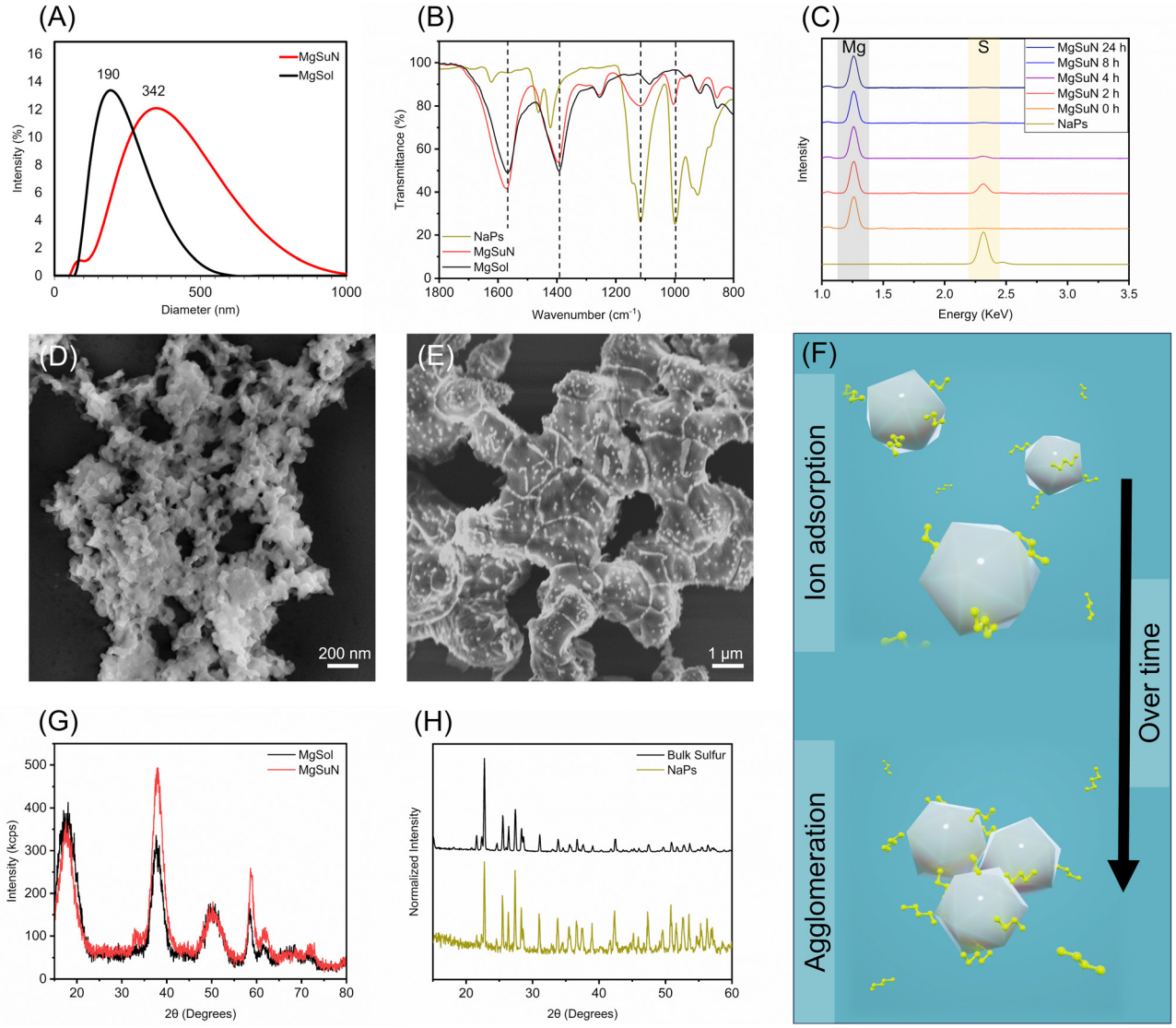

Fig. 1 (A) Hydrodynamic diameter of MgSuN (red curve) and MgSol (black curve). (B) FTIR of NaPs, MgSuN, and MgSol. (C) EDS spectra of purified NaPs and of MgSuN samples after stirring for 0 h, 2 h, 4 h, 8 h, and 24 h. (D) SEM image of MgSuN (800 ppm of Mg and 400 ppm of S) after 24 hours of stirring. (E) SEM image of NaPs after 24 hours of stirring. (G and H) Diffractograms obtained from the precipitate of (G) MgSol, MgSuN and (H) NaPs, after stirring for 24 hours at 800 ppm S, 800 ppm Mg, or 600 ppm Mg and 200 ppm S, respectively. (F) Schematics of the proposed interactions between MgSol and NaPs.

represented in Fig. 1F. This process is initiated by the polysulfide ions adsorption onto the surface of the nanoparticles, leading over time to the agglomeration of the particles, leading to an increase in hydrodynamic size. In an aqueous environment, this behavior slows down the degradation of the polysulfide ions and impacts $Mg(OH)_2$ dissolution. The latter is supported by the XRD analysis showcasing the differences in the relative intensity of the (001), (101) and (110) reflections between MgSuN and MgSol.

Theoretical analysis

Based on previous literature,[73] the (001) facet of $Mg(OH)_2$ is expected to be predominant for MgSol nanoparticles in solution. The interaction between sodium polysulfides and the (001) surface facet of $Mg(OH)_2$ was thus studied with DFT (Fig. S11 and S12).

The speciation of S_x^{2-} at a basic pH is shown to vary from x = 1 to 8, with the S_4^{2-}, S_5^{2-}, and S_6^{2-} ones to be most dominant in an aqueous environment at ambient conditions.[43] However, estimating the binding of a charged system in an aqueous environment can give rise to spurious electrostatic effects. Hence, in the present study, the geometries of these polysulfides in isolation (Fig. S11(A–H)) and upon adsorption onto the hydroxide surface have been investigated (Fig. 2B). The structures of these polysulfides are shown to be ordered when unadsorbed. As the chain length increases, the clustering is shared between the Na^+ ions. This is exhibited by equatorial arrangement of the S around the cationic moiety. The S–

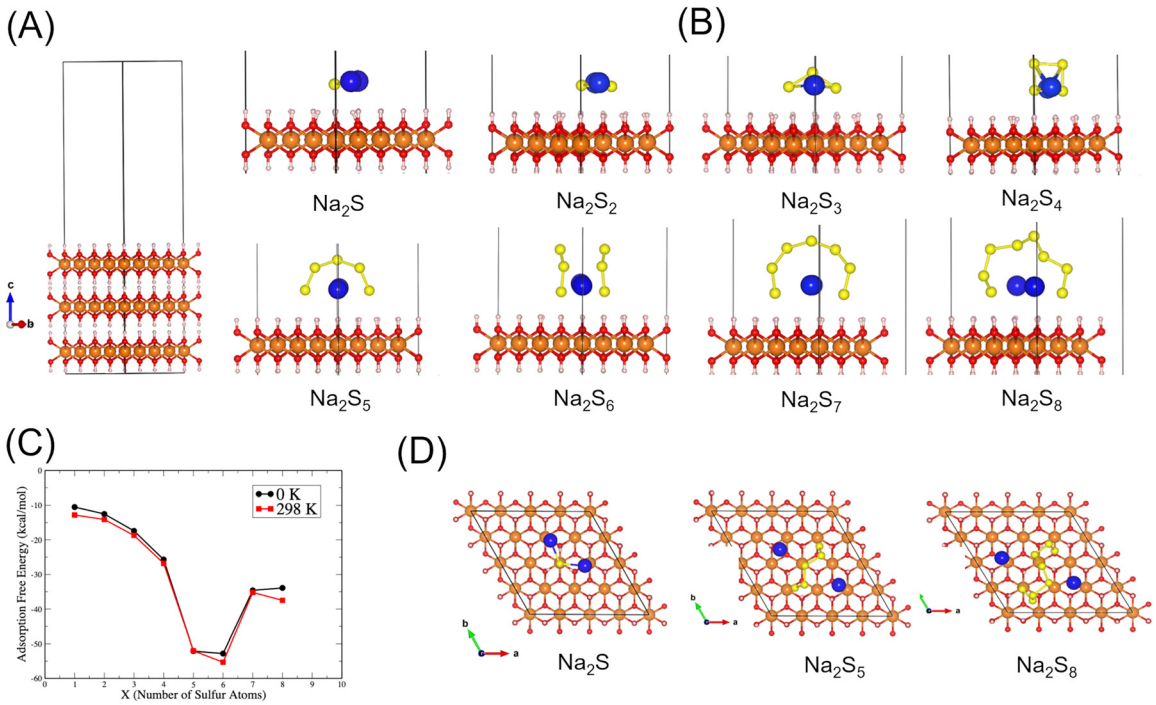

Fig. 2 (A) Clean $Mg(OH)_2$ surface optimized (B) side views of the surface adsorbate model with the substrates ranging for all sodium polysulfides considered (Na_2S_x) (x = 1–8) (C) adsorption free energies computed at 0 and 298 K (D) side views of the surface adsorbate models of Na_2S, Na_2S_5 and Na_2S_8.

S bond lengths range from 1.96–2.32 Å across the species, which falls close to former works published with regards to both lithium and sodium polysulfides.[74,75] Upon adsorption, it is observed that as the chain length of the sulfur atoms is increased, a crown shaped conformation is favored on the surface of $Mg(OH)_2$ (Fig. 2B & D). The sulfur atoms conveniently arrange themselves around the cations remaining stable. Energetically, the adsorption free energies range from −10.5 to −52.8 kcal mol^{-1} at 0 K and −12.8 to −55.3 kcal mol^{-1} when corrected for entropic contributions at 298.15 K. This suggests that the binding of Na_2S_x on the c-axis surface facet of $Mg(OH)_2$ is rather stable and enthalpically driven irrespective of the size of the polysulfide. Moreover, Na_2S_5 and Na_2S_6 bind most strongly to the surface of the hydroxide. A recent study on their binding on Ti containing MXenes also reports strong adsorption affinity in excess of about −46 kcal mol^{-1} (2 eV) on an O-exposed surface.[74] The formation of polysulfide chains is posited by S–S bonds ranging from 2.02–2.14 Å atop the stable hydrogen-rich surface. It is also observed that the Na ions reside about 2.1–2.4 Å above the top layer of $Mg(OH)_2$ to further augment the favourability of the binding process. Our investigation points towards the potential ability of $Mg(OH)_2$ in preventing the dissolution of Na_2S_x in an aqueous environment, echoing the conclusions regarding polysulfide stability in the Material characterization section.

Overall, the theoretical evidence supports the hypothesis that sodium polysulfides adsorb on the $Mg(OH)_2$ surfaces at ambient conditions. The presence of a stable polysulfide MgSol complex is shown to be plausible and in agreement with the material changes in hydrodynamic size, FTIR spectra, and EDS spectra.

Radical scavenging assessment

Polysulfide ions are highly reactive and have been shown to scavenge radicals from DPPH.[76] However, their adsorption on the surface of $Mg(OH)_2$ nanoparticles might affect their activity and degradation. A radical scavenging assay was conducted to evaluate the stability of NaPs in MgSuN over 24 hours. Upon the addition of DPPH to NaPs, an absorbance maximum shift from 540 nm to 430 nm was observed (Fig. 3A) in the UV-Vis spectra, corresponding to a color change from purple to yellow in the cuvette, as shown in Fig. 3G. After 2 hours of mixing, the absorbance at 430 nm from the sample containing no MgSol was reduced significantly, while the absorbance of the sample containing 60 and 180 ppm of Mg remained relatively constant (Fig. 3B).

Following 8 hours, the sample containing no MgSol lost all its scavenging potential, while the samples containing MgSol demonstrated different degrees of absorbance (Fig. 3C), suggesting reactivity. A representative image can be observed in Fig. 3G. Similarly, after 16 hours, the absorbance of the samples containing only NaPs and containing 20 ppm Mg, reverted completely to an absorption centered at 540 nm. However, the samples containing 60 and 180 ppm Mg of MgSol were still absorbing at 430 nm (Fig. 3D). After 24 hours,

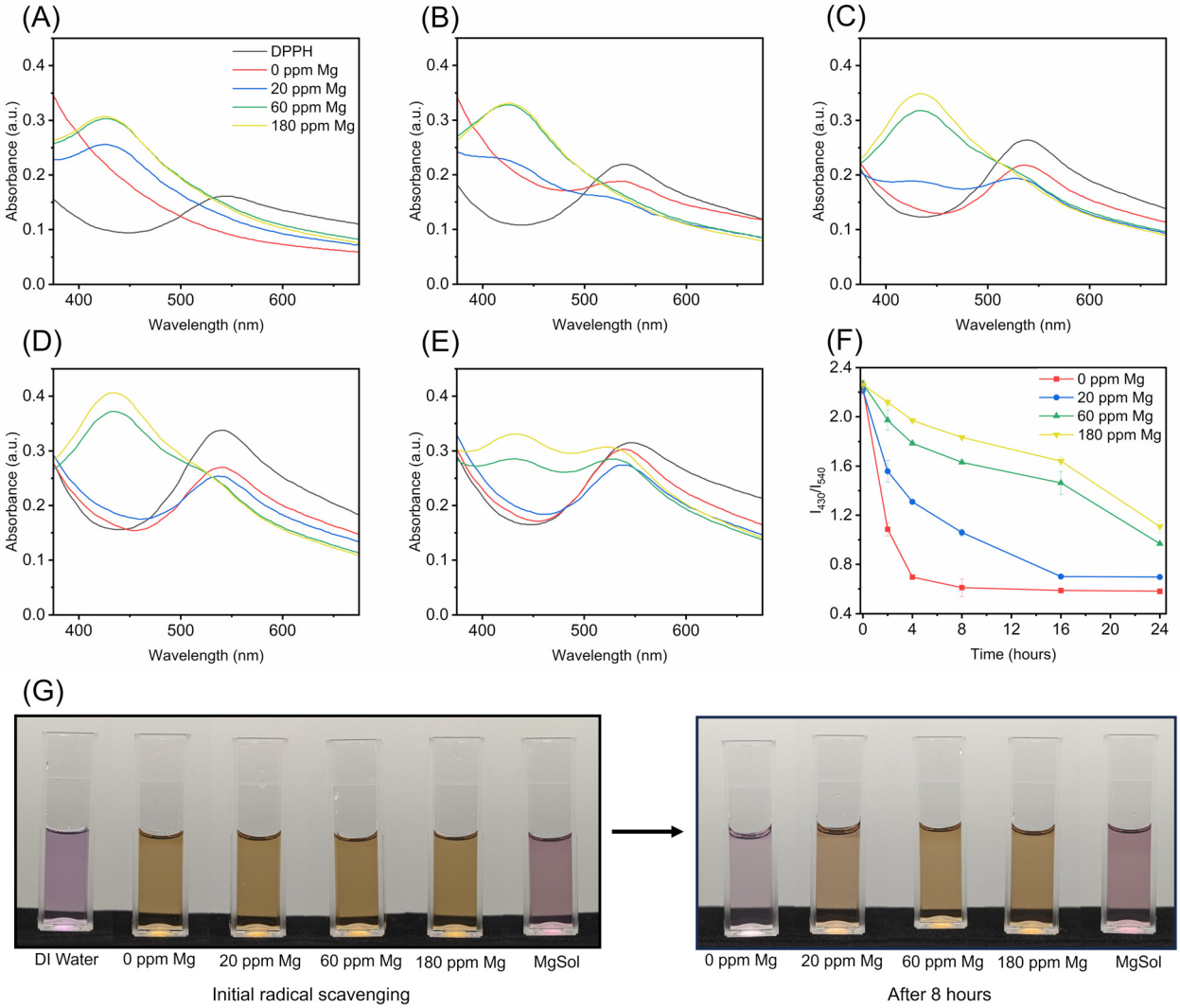

Fig. 3 UV-Vis spectra collected from MgSuN samples of varying concentrations mixed with DPPH after (A) 0 hour, (B) 2 hours, (C) 8 hours, (D) 16 hours, and (E) 24 hours of stirring. (F) Ratiometric analysis of the absorbance at 430 nm/absorbance at 540 nm, for the different concentrations of MgSuN. (G) Representative digital image showing the difference in radical scavenging potential of MgSuN at different concentration before and after 8 hours of stirring after dilution.

they exhibited similar light absorption at both 540 nm and 430 nm (Fig. 3E). As a result, it is inferred that MgSol has a concentration dependent effect on the absorption at 430 nm over time, with high MgSol concentration leading to higher radical scavenging activity. The degradation of NaPs over time can be described by plotting $I_{540\ \mathrm{nm}}/I_{430\ \mathrm{nm}}$ (Fig. 3F). In absence of Mg (red curve, Fig. 3F), the ratio dropped to over 50% of the initial value in less than 2 hours. Increasing the concentration of MgSol delayed the degradation of polysulfides over time, with the higher concentrations retaining half of NaPs' scavenging potential for a period 12 times longer than polysulfide ions on their own. This is most likely due to the adsorption of the polysulfide ions on the surface of the Mg $(OH)_2$ nanoparticles that possess a local basic environment, preventing the disproportionation of polysulfides, hence extending the lifetime of these species, after dilution.

Antimicrobial properties assessment

The antimicrobial potency of MgSuN was evaluated using a checkerboard assay (Fig. 4A). Overall, the results demonstrate that MgSuN possesses enhanced antimicrobial potency compared to its individual components. Concentrations below the black curve in Fig. 4A and B represent antimicrobial combinations that possess an additive effect. From the heatmap in Fig. 4A corresponding to the MIC assay, it is notable that treatment with 256 ppm Mg/0.5 ppm S and 64 ppm Mg/1 ppm S inhibited the growth of *Xac* at lower concentrations compared to the MIC of the individual antimicrobials. The FIC of these mixtures was calculated to be 0.75 and 0.625, respectively, corresponding to additive inhibitory properties. On the other hand, the MBC map in Fig. 4B shows that treatments at 64 ppm Mg/4 ppm S and 64 ppm Mg/2 ppm S prevented bac-

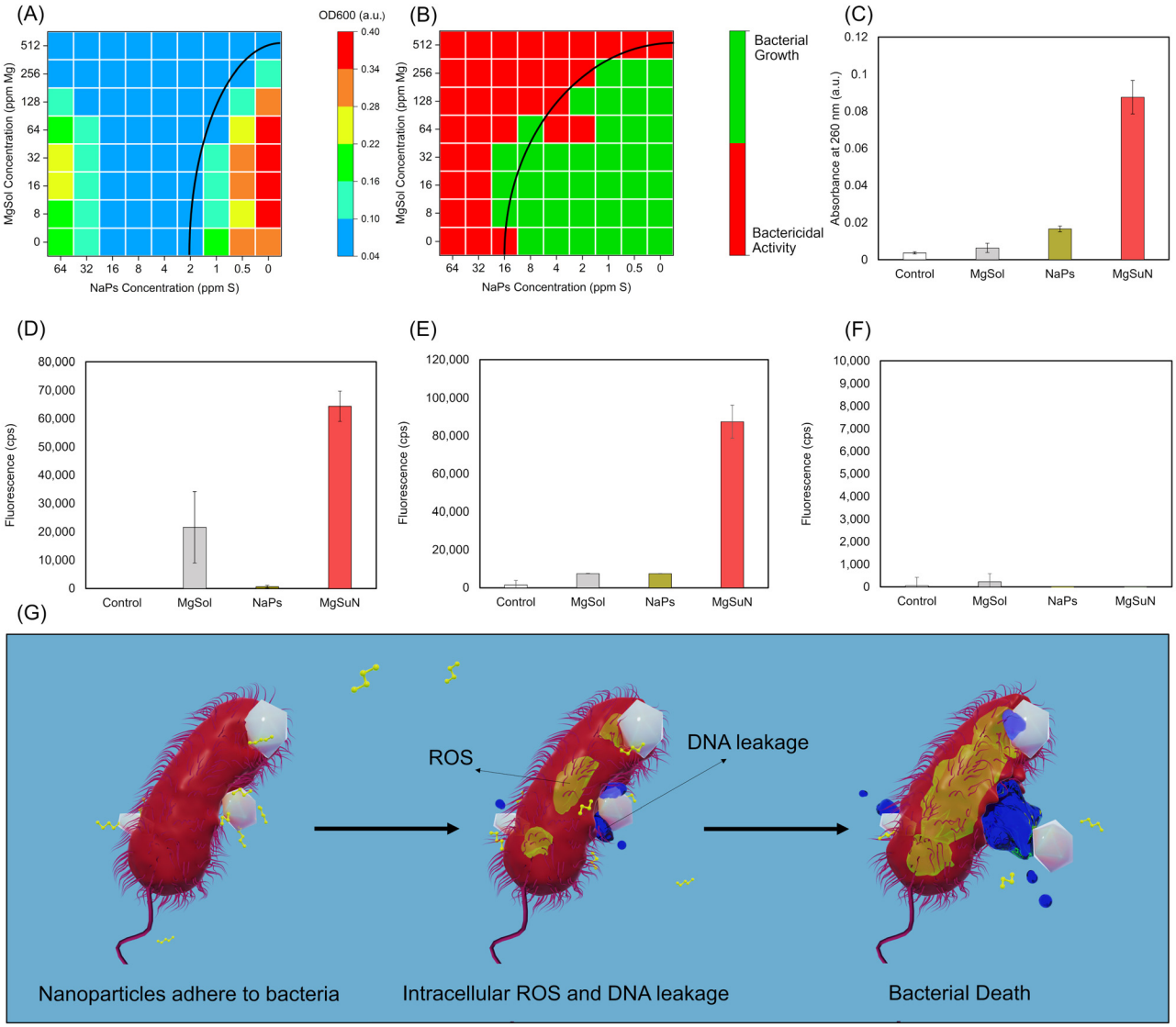

Fig. 4 Heatmaps constructed from (A) the checkerboard assay and (B) the MBC assay against *Xac*. The black curve represents the theoretical behavior of a mixture demonstrating additive effect. (C) Absorbance of *Xac* exposed to MgSol, NaPs, and MgSuN at 260 nm. An increase in absorbance correlates with DNA leakage from the bacteria. (D) Fluorescence of the treated cells exposed to DCFH-DA, demonstrating intracellular ROS activity. (E) Fluorescence of the treated cells exposed to red peroxide reagent, showing the presence of intracellular H_2O_2. (F) Fluorescence of the treated cells exposed to HPF, indicating intracellular hydroxyl radical activity. (G) Schematic depicting the nanoparticle's proposed role in bacterial death.

terial colony formation. The FBC of the treatments was 0.375 and 0.25, respectively, corresponding to synergistic efficacy.

An increase in the OD600 (Fig. 4A) in the treatments containing 128–0 ppm Mg when NaPs was applied at 64–32 ppm S was noted, but no bacterial colonies were formed when bacteria from these wells were plated (Fig. 4B). This suggests that the increase in OD600 resulted from the treatments and not bacterial growth. This was corroborated by combining MgSol and NaPs at different ratios and observing the visible changes in opacity after 24 hours of mixing (Fig. S2). This is in agreement with the behavior of NaPs in solution, and the prolonged reactivity afforded by adsorbing NaPs on MgSol.

MgSol[24] and other nanoparticle bactericides[77–79] have been previously reported to have similar efficacy against different *Xanthomonas* species. Therefore, MgSuN was tested against *Xp*. Synergistic antimicrobial activity was observed at 64 ppm Mg/2 ppm S in this case (Fig. S5A). Similar antimicrobial potency was documented in stable synthetic organic polysulfides against other *Xanthomonas* pathogens.[80,81] This emphasizes the benefits of stabilizing the sulfur motifs and their potency against other pathogens in the *Xanthomonas* genus. On the other hand, NaPs and MgSol partially inhibited Ps at 64 ppm S and 512 ppm Mg, respectively, with MgSuN only showing additive behaviour by inhibiting the bacteria at 256 ppm Mg/1 ppm S (Fig. S5B). Previously, Xu *et al.* stabilized polysulfides by converting natural organosulfur compounds to $Fe_{1-x}S$ and Fe_3S_4 nanoparticles,[76] while Dop *et al.* stabilized polysulfides by synthesizing vulcanized polymer nanoparticles.[82] Similar

materials could be adapted for future studies to tackle different pathogens. Altogether, our results and these studies show the limitations and potential of polysulfide-based biocides for managing other plant diseases.

Another interesting aspect of these results is the eight-fold difference between the MIC and MBC against *Xac*. It is surmised that this difference is due to polysulfide degrading over time.[41–43] Due to chemical reactions (1) and (2), the concentration of polysulfide ions decreases over time, diminishing its bactericidal activity. Some of the degradation products, such as hydrogen sulfide, may possess biocidal action, but some *Xanthomonas* subspecies reduce hydrogen sulfide.[83] Consequently, the prolonged chemical stability of polysulfide adsorbed on MgSol particles allows for effective concentrations persisting long enough to induce irreversible damage to cell respiration and exert bactericidal activity. Considering this hypothesis, the antimicrobial activity of MgSuN was assessed at different times after dilution (Fig. S4). MgSuN at 16 ppm Mg reduced the MIC by one dilution stage after 2 and 8 hours, compared to NaPs (Fig. S4C & D). Similar results were also identified when 64 or 128 ppm Mg were supplied, in which the MIC at all tested times was reduced (Fig. S4A & B). The findings support the hypothesis that MgSol fosters a nano-mediated stabilization of polysulfide ions leading to an improved antimicrobial activity.

To further understand the mechanisms underlying MgSuN's antimicrobial efficacy, DNA leakage, and intracellular ROS production in *Xac* (Fig. 4C–F) were assessed. Magnesium-based nanomaterials are known to exhibit bactericidal activity, which is generally attributed to physical damage to the cellular membrane, leading to nucleic acid leakage and ROS production.[24,84–87] MgSuN at the synergistic concentration (64 ppm Mg/2 ppm S) elevated the characteristic absorbance of DNA (260 nm), compared to the individual components and untreated control, evidencing substantial nucleic acid leakage from cellular damage. In addition, the results from the intracellular ROS assay demonstrated heightened fluorescence in cells treated with the MgSol and MgSuN, suggesting elevated ROS levels relative to NaPs and the untreated cells. Nevertheless, on average, MgSuN enhanced intracellular ROS by 298% over MgSol, indicating that the combinatorial treatment exacerbates the bacterial metabolism significantly. Additionally, specific fluorescent probes were utilized to identify the ROS species present inside the cells. None of the treatments impacted the production of intracellular hydroxyl radicals, as shown by the lack of HPF fluorescence after treatment, compared to the untreated bacteria. In contrast, Fig. 4E demonstrates that at synergistic concentrations of MgSuN, peroxide concentrations significantly increases unlike with other treatments. Hence, build-up of intracellular peroxide upon treatment with MgSuN at 64 ppm Mg/2 ppm S contributes to its enhanced bactericidal activity.

While MgSol at 64 ppm Mg caused some intracellular ROS (Fig. 4D), it did not inhibit bacterial growth. In contrast, polysulfides are expected to impair electron transport and disrupt sulfur homeostasis by interfering with hydrogen sulfide production.[40] Once polysulfide ions are uptaken by microbes, they react with the mitochondrial respiratory complex, inhibiting electron flux and exerting broad-spectrum antimicrobial effects.[40] Additionally, it is well-documented that polysulfide solutions generate excess hydrogen sulfide, which can cause protein persulfidation, impacting sulfur homeostasis.[88,89] Considering this, it is likely that MgSuN engages multiple metabolic pathways simultaneously, resulting in additive inhibitory effects at most concentrations and synergistic bactericidal activity at specific ratios. Overall, these results corroborate that MgSuN induces significant oxidative stress through intracellular peroxide, which leads to enhanced cellular membrane disruption, and ultimately causes cellular death as depicted in Fig. 4G.

Plant-MgSuN interactions

To assess the phytotoxicity of the nanoformulation to vegetable crops, 6-week old commercial pepper and tomato plants were sprayed with 25 mL of the formulation at different concentrations and then incubated for 3 days in a growth chamber (Fig. 5A). The leaves of the treated pepper plant leaves are shown in Fig. 5B–G. Most pepper leaves did not show any necrotic lesions or yellowing despite there being several visible spots of chemical residue. Similar observations were recorded for the phytotoxicity assessment in tomato plants (Fig. 5I & S6). The severity of the phytotoxicity was recorded for all leaves on the treated bell peppers and tomato plants and their frequency was compiled in Fig. 5H & I. The results demonstrate that MgSuN does not cause any phytotoxicity on either pepper or tomato. Less than 6.7% of bell pepper leaves were observed to have moderate damage, compared to 14.9% of tomato leaves that showed minimal toxicity. It is worth noting that in formulations where MgSol and NaPs were combined in equal concentrations, the average percentage of affected leaves was the lowest, with 0% and 5.5% for bell peppers and tomato leaves, respectively. These results were comparable to the DI control on both crops and correlated with the findings from the radical scavenging assay, in which MgSol mitigated the reactivity of the polysulfide ions, hence reducing the phytotoxicity caused by NaPs. For pepper plants, high concentrations of MgSol increased the average percentage of affected leaves to 23.2%, thus it is important to use the right ratio of MgSol when formulating MgSuN.

It has been reported that vegetable crops, such as peppers and tomatoes, can transmit *Xanthomonas* pathogens to the next generation of crops through seeds.[4,90,91] Since MgSuN exhibited considerable antimicrobial potency *in vitro*, its phytotoxicity was evaluated on pepper seeds in view of preventing seed-borne disease and decontaminating seeds. For this, pepper seeds were primed with MgSuN, sown, and the timing at which new seedlings emerged from the soil was monitored. The results, presented in Fig. S7, show that on average all treatments reduced seed germination at the 10 day mark, as compared to the DI control and normally sown seeds, whereas no significant difference could be noted at the 20 or 30 day mark. Histograms (Fig. 5J) were constructed using the number of

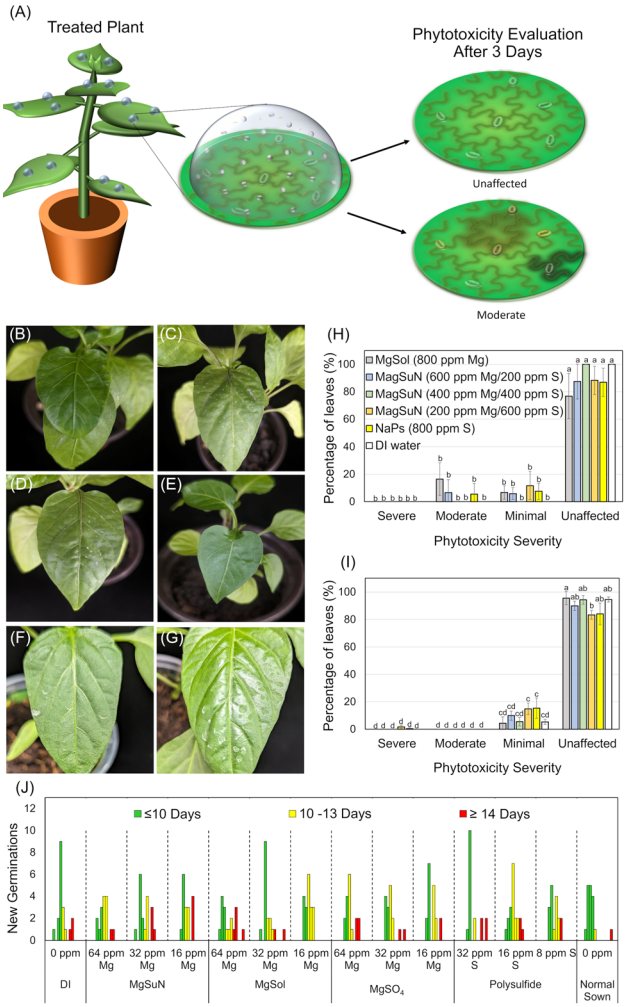

Fig. 5 Schematic representing the agrochemical treatments drying process on the leaf surface and the onset of phytotoxicity (A). Digital photographs of bell pepper plants sprayed with MgSuN at (B) 600 ppm S and 200 ppm Mg, (C) 600 ppm Mg and 200 ppm S, (D) 400 ppm Mg and 400 ppm S, (E) DI, (F) 800 ppm S and (G) 800 ppm Mg. All Mg content originates from MgSol, while all S content originates from NaPs. The images show the health of the foliage as well as the chemical residue on the surface of the leaves. Phytotoxicity assessment of (H) bell pepper and (I) tomato plants sprayed with different concentrations of MgSuN. Error bars represent standard deviation. Different letters (a–d) were assigned to statistically significant groups according to a Tukey's *post hoc* analysis (p = 0.05). (J) Histograms of new seedling emergence from bell pepper seeds primed with different concentrations of MgSuN.

new seedling emergence per day after sowing. The histograms show that for the DI control and the normal sown seeds, new seedling emergence occurs in a bimodal distribution, with most seedlings emerging under 10 days (green bars in Fig. 5J). However, when the seeds were primed the difference between these distributions was largely diminished, causing most new germinations to occur between the 10th and 20th day (yellow and red bars). Therefore, even though no treatment caused the final germination percentage to be less than 80% there was a pronounced delay in the onset of germination. Given that MgSol, NaPs, MgSuN, and $MgSO_4$ affected the seeds similarly, it suggests that this effect is caused by the ionic content rather than specific phytotoxicity pathways. Furthermore, these findings imply that MgSuN causes no significant toxicity to pepper seeds at concentrations under 64 ppm Mg/32 ppm S, which corresponds to formulations that exhibit bactericidal activity.

Given its excellent bactericidal activity and low disruption of seed germination, MgSuN demonstrates potential as a seed treatment in nurseries to control seed-borne pathogens. However, more in depth studies need to be performed to assess the efficiency of MgSuN for the generational transmission of pathogens on different plant systems.

Moreover, the characteristics of chemical residues on the leaves were studied. The ratio of MgSol to NaPs seemed to impact the deposits as shown in the SEM images for each of the treatments (Fig. 6B–G). Formulations containing MgSol alone or mixed in higher concentrations than NaPs produced a thicker residue exhibiting cracks and prone to flaking off. On the other hand, formulations with equal or higher concentrations of NaPs compared to MgSol produced residue with uniform leaf coverage, with similar observations made on tomato leaves (Fig. S8).

The elemental composition of the residues was mapped using EDS (Fig. S9), showing an even distribution of Mg, S, and Na on plants treated with MgSuN. Plants treated with only MgSol or NaPs did not display high intensity for S or Mg, respectively, as opposed to plants treated with MgSuN (Fig. S10). These results demonstrate that MgSuN distributes Mg and S uniformly on the leaf, even after drying, which is vital to ensure that both antimicrobials will be in contact with the pathogen at the same time. The co-exposure of microbes to NaPs and MgSol increases the likelihood of the additive/synergistic activity observed in the antimicrobial studies. On the other hand, this interaction between materials enhanced the biocompatibility and provided MgSuN at 400 ppm Mg/400 ppm S to be comparable to DI water in terms of phytotoxicity. It is valuable to control polysulfide's phytotoxicity because it is known to reduce pollen tube viability.[92] Lime sulfur, containing calcium polysulfide, is used in apple orchards for flower thinning and fruit quality enhancement, with studies indicating that other chemicals can enhance its effectiveness.[93,94] Exploring MgSol's impact on polysulfide thinning properties is necessary, as flower thinning, though less common in vegetable crops, has been shown to improve fruit quality without reducing yield.[95,96]

Next, rainfastness and total Mg content of the chemical residues were assessed through a water immersion method, as shown in Fig. 6A. Even though MgSuN residues were more evenly distributed, 60–79% of the Mg was released during the first water wash for all treatments (Fig. 6H & I). Interestingly, MgSuN at 600 ppm Mg /200 ppm S retained on average 242.2 μg of Mg on the surface of the leaf, which was found to be significantly more than MgSol at 800 ppm Mg with only 119.6 μg accumulated on average. Furthermore, MgSol's deposition was found to be statistically similar to that of MgSuN at 400 ppm Mg/200 ppm S. This demonstrates that NaPs does not improve the water-resistance of the formulation but increases the total amount of MgSol that is retained on the surface of the leaf (Fig. 6J).

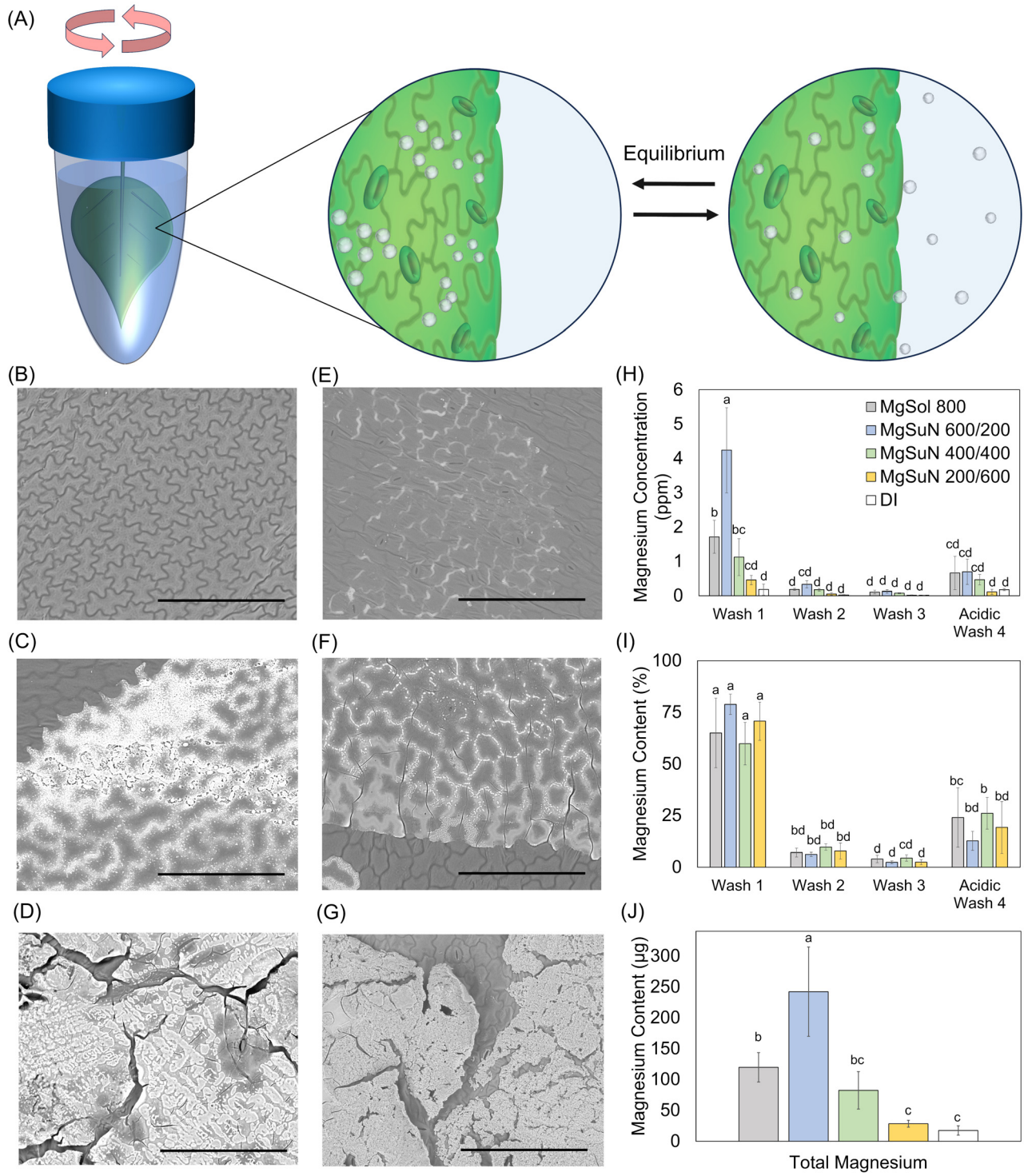

Fig. 6 (A) Schematic representation of the material's leaf adherence when immersed in water. SEM images of the chemical residues on the surface of the leaves of bell pepper plants treated with (B) DI water, (C) MgSuN at 600 ppm S and 200 ppm Mg, (D) 600 ppm Mg and 200 ppm S, (E) 800 ppm S, (F) 400 ppm Mg and 400 ppm S, and (G) 800 ppm Mg. Scale bars are set to 200 μm. Rainfastness assessment of the residues on the surface of the leaves of bell pepper plants. The assessment is presented as (H) magnesium concentration in the wash solutions, (I) percentage of magnesium content that was present in each wash, and (J) the total mass of magnesium present in each wash. The error bars represent the standard deviation. Different letters (a–d) were assigned to statistically significant groups according to a Tukey's *post hoc* analysis (p = 0.05).

Usually for pesticides, more material deposition results in better crop protection and less runoff.[97] For this reason, adjuvants and specialized nozzles are often recommended to enhance pesticide retention and coverage.[98,99] Still, higher deposition efficiency was achieved by combining two active ingredients without the need for surfactants or equipment. From the SEM images, it is evident that mixing at least 400 ppm S is necessary to achieve a uniform deposition, akin to that of a polymeric film. Polysulfides films have been shown to generate small sulfur coatings with antimicrobial properties,[100–102] suggesting that MgSuN will protect against pathogens even in the dry state.

Inorganic biocides, like MgSuN, have the potential to not only combat pathogens but also to provide nutritional benefits, as magnesium (Mg) and sulfur (S) are essential macronutrients for plants.[103] While this study did not focus on MgSuN's nutritional effects, Mg and S have been shown to improve crop yields[104–108] and enhance stress responses.[88,89] Additionally, polysulfides have been shown to form sulfur nanoparticles through reaction (2),[102,109] which have antifungal,[110] antibacterial,[111] and disease resistance-inducing properties.[112–114] Similarly, MgO nanoparticles have been reported to induce systemic resistance in plants.[115] Future studies will investigate MgSuN's impact on plant hormones and pathogenesis-related proteins to understand its agricultural potential further.

Conclusions

In summary, this work investigated the antimicrobial properties of nanodelivered NaPs (MgSuN) as a sustainable approach to combat *Xanthomonas* pathogens in vegetable crops. It was determined that MgSol adsorbed polysulfide ions upon addition of NaPs, which led to an increase in hydrodynamic size (190 nm to 342 nm) due to particle agglomeration. Over time, this prevented the formation of micron-sized α-sulfur stemming from polysulfide degradation. Theoretical analysis of the system demonstrated that physisorption between the polysulfide ions and the (001) $Mg(OH)_2$ surface is thermodynamically favored. Colorimetric radical scavenging assays demonstrated that polysulfide ions in MgSuN degraded slower and scavenged radicals for a period 12 times longer than NaPs alone. This interaction is hypothesized to be the main mechanism through which MgSol affects NaPs' biological interactions.

By leveraging the nano-mediated stabilization of polysulfide ions with $Mg(OH)_2$ nanoparticles, MgSuN significantly enhanced the biocidal efficacy of sodium polysulfide. At specific ratios, the formulation demonstrated synergistic activity through an 8-fold improvement in bactericidal potency against the model pathogen *Xac* and *Xp*. Mechanistic studies revealed that MgSuN's improved antimicrobial action stems from a 297.6% increase of intracellular ROS, which afforded enhanced disruption of cellular membranes. A peroxide-reactive fluorescent molecular probe confirmed that MgSuN treated bacteria experience a substantial increase in intracellular peroxide. This provides valuable insights into the materials' mode of action and shows the potential of bioactive delivery systems, like MgSol, to boost the potency of agrochemicals.

Additionally, the combination in equal concentrations of MgSol and NaPs, showed increased biocompatibility by reducing the average incidence of leaf burn to a level comparable with the untreated control. The chemical residues on treated leaves varied with NaPs and MgSol concentration ratios. MgSuN (600 ppm Mg/200 ppm S) resulted in the deposition of significantly more magnesium on leaf surfaces than MgSol (800 ppm Mg). When used to prime pepper seeds by exposing them for 24 hours, germination rates after 20 days were not affected, suggesting a new way to reduce generational transmission.

Often nanopesticides are framed as substitutes or better alternatives to already existing active ingredients. Although many nanomaterials have been estimated to be more effective than their bulk counterparts, there is limited information regarding their safety and environmental fate. On the other hand, the first record of lime sulfur, a polysulfide biocide, dates to 1833.[39] After 190 years, lime sulfur has mostly been replaced by synthetic small molecules, but its cytotoxicity and ecotoxicity are well understood.[39,40] By delivering this antiquated pesticide with nano $Mg(OH)_2$ it is possible to reuse it more effectively. Utilizing well-understood active ingredients can be more favorable than designing new molecules and establishing their effectiveness and toxicology. In general, this work demonstrates the potential of nanodelivery systems to enhance the effectiveness of conventional, well-established active ingredients through synergistic integration. Although the ecotoxicity and biosafety of MgSuN are yet to be evaluated, its potential environmental impact could be predicted based on a wealth of existing data on $Mg(OH)_2$ and polysulfides.

Considering all the findings, the nanodelivery of NaPs *via* MgSol resulted in multiple benefits such as improved antimicrobial potency, phytotoxicity reduction, and prolonged agrochemical retention on the surface of the leaf. The enhancement of these performance parameters suggests that MgSuN would be a better crop disease management tool for vegetable crops than its individual components.

Author contributions

Conceptualization, J. P., E. D., J. R., and S. S.; investigation, J. P., J. R., E. D, M. D., P. M., A. B., B. D., and A. L.; methodology, J. P., E. D., A. B. and B. D.; data curation, J. P.; visualization, J. P. and A. B.; formal analysis, J. P. and E. D.; writing—original draft preparation, J. P.; writing—review and editing J. P., J. R., E. D, M. D., P. M., A. L., A. B., S. Z., B. D., L. T., and S. S.; resources, S. S.; supervision, S. Z., L. T., and S. S.; project administration, S. S.

Conflicts of interest

S. S. has submitted patent application US20200120937A1 based on previous work on MgSol. There are no other conflicts to declare.

Data availability

All data relevant to this article are provided either within the main manuscript or in the SI.

Supporting Fig. 1 (Fig. S1). Raman and UV-Vis spectra of sodium polysulfide.

Supporting Fig. 2 (Fig. S2). Images of MgSuN at different ratios after 24 hours.

Supporting Fig. 3 (Fig. S3). MIC of NaPs combined with 0, 16, 64 and 128 ppm of Mg.

Supporting Fig. 4 (Fig. S4). Checkerboard assessment of MgSuN on *Xp* and *Ps*.

Supporting Fig. 5 (Fig. S5). Phytotoxicity on tomato leaves.

Supporting Fig. 6 (Fig. S6). Seed emergence percentage of primed pepper seeds.

Supporting Fig. 7 (Fig. S7). SEM of chemical residue on tomato leaves.

Supporting Fig. 8 (Fig. S8). EDS map of chemical residue on pepper leaves.

Supporting Fig. 9 (Fig. S9). EDS spectrum of chemical residue on pepper leaves.

Supporting Fig. 10 (Fig. S10). Optimized structure of the $Mg(OH)_2$ (001) slab model and Initial surface-adsorbate geometry for DFT calculations consisting of polysulfide ions.

Supporting Fig. 11 (Fig. S11). Optimized surface-adsorbate geometry from DFT calculations. See DOI: **https://doi.org/10.1039/d5nr03087k**.

Acknowledgements

The authors would like to acknowledge the help the Santra group members at setting up the greenhouse studies. The authors especially thank Andrea Bardales for her help in quantifying seed emergence. The Material Characterization Facility of the University of Central Florida – Advanced Materials Processing and Analysis Center is acknowledged for providing the SEM facility and technical support. This work was supported by the USDA National Institute of Food and Agriculture, Specialty Crops Research Initiative, grant no. 2019-51181-30010. The team acknowledges NSF MRI DMR-1920050 for the Horiba Raman confocal microscope system.

References

1 P. M. M. Martins, M. V. Merfa, M. A. Takita and A. A. De Souza, *Front. Microbiol.*, 2018, **9**, 1099.
2 S. Timilsina, N. Potnis, E. A. Newberry, P. Liyanapathiranage, F. Iruegas-Bocardo, F. F. White, E. M. Goss and J. B. Jones, *Nat. Rev. Microbiol.*, 2020, **18**, 415–427.
3 J. Mansfield, S. Genin, S. Magori, V. Citovsky, M. Sriariyanum, P. Ronald, M. Dow, V. Verdier, S. V. Beer, M. A. Machado, I. Toth, G. Salmond and G. D. Foster, *Mol. Plant Pathol.*, 2012, **13**, 614–629.
4 N. W. G. Chen, M. Ruh, A. Darrasse, J. Foucher, M. Briand, J. Costa, D. J. Studholme and M. A. Jacques, *Mol. Plant Pathol.*, 2021, **22**, 1464–1480.
5 H. Koenraadt, B. van Betteray, R. Germain, G. Hiddink, J. B. Jones, J. Oosterhof, A. Rijlaarsdam, P. Roorda and B. Woudt, presented in part at the II International Symposium of Tomato Diseases, 2009.
6 I. S. Myung, S. Y. Moon, I. H. Jeong, S. W. Lee, Y. H. Lee and H. S. Shim, *Plant Dis.*, 2010, **94**, 790–790.
7 E. Stefani, *J. Plant Pathol.*, 2010, S99–S103.
8 E. Osdaghi, J. B. Jones, A. Sharma, E. M. Goss, P. Abrahamian, E. A. Newberry, N. Potnis, R. Carvalho, M. Choudhary and M. L. Paret, *Mol. Plant Pathol.*, 2021, **22**, 1500.
9 D. Tilman, C. Balzer, J. Hill and B. L. Befort, *Proc. Natl. Acad. Sci. U. S. A.*, 2011, **108**, 20260–20264.
10 M. van Dijk, T. Morley, M. L. Rau and Y. Saghai, *Nat. Food*, 2021, **2**, 494–501.
11 M. Carvajal-Yepes, K. Cardwell, A. Nelson, K. A. Garrett, B. Giovani, D. G. O. Saunders, S. Kamoun, J. P. Legg, V. Verdier, J. Lessel, R. A. Neher, R. Day, P. Pardey, M. L. Gullino, A. R. Records, B. Bextine, J. E. Leach, S. Staiger and J. Tohme, *Science*, 2019, **364**, 1237–1239.
12 S. Savary, L. Willocquet, S. J. Pethybridge, P. Esker, N. McRoberts and A. Nelson, *Nat. Ecol. Evol.*, 2019, **3**, 430–439.
13 J. M. Klein-Gordon, Y. R. Xing, K. A. Garrett, P. Abrahamian, M. L. Paret, G. V. Minsavage, A. L. Strayer-Scherer, J. C. Fulton, S. Timilsina, J. B. Jones, E. M. Goss and G. E. Vallad, *Phytopathology*, 2021, **111**, 1029–1041.
14 E. Shahbaz, M. Ali, M. Shafiq, M. Atiq, M. Hussain, R. M. Balal, A. Sarkhosh, F. Alferez, S. Sadiq and M. A. Shahid, *Plants*, 2022, **12**, 123.
15 J. Fayette, P. D. Roberts, K. L. Pernezny and J. B. Jones, *Crop Prot.*, 2012, **31**, 107–112.
16 M. Šević, K. Gašić, M. Ignjatov, M. Mijatović, A. Prokić and A. Obradović, *Crop Prot.*, 2019, **119**, 46–51.
17 A. Herbert, C. N. Hancock, B. Cox, G. Schnabel, D. Moreno, R. Carvalho, J. Jones, M. Paret, X. Q. Geng and H. H. Wang, *Front. Microbiol.*, 2022, **13**, 821808.
18 J. Garita–Cambronero, A. Palacio–Bielsa and J. Cubero, *Mol. Plant Pathol.*, 2018, **19**, 2053–2065.
19 A. Subedi, G. V. Minsavage, J. B. Jones, E. M. Goss and P. D. Roberts, *Plant Dis.*, 2023, **107**, 2978–2985.
20 A. Soto-Caro, G. E. Vallad, K. V. Xavier, P. Abrahamian, F. Wu and Z. Guan, *Agronomy*, 2023, **13**, 972.
21 M. Kah and T. Hofmann, *Environ. Int.*, 2014, **63**, 224–235.
22 D. J. Wang, N. B. Saleh, A. Byro, R. Zepp, E. Sahle-Demessie, T. P. Luxton, K. T. Ho, R. M. Burgess, M. Flury, J. C. White and C. M. Su, *Nat. Nanotechnol.*, 2022, **17**, 347–360.
23 N. Y. T. Nguyen, N. Grelling, C. L. Wetteland, R. Rosario and H. Liu, *Sci. Rep.*, 2018, **8**, 16260.
24 Z. Huang, P. Rajasekaran, A. Ozcan and S. Santra, *J. Agric. Food Chem.*, 2018, **66**, 8679–8686.
25 L. Cai, J. N. Chen, Z. W. Liu, H. C. Wang, H. K. Yang and W. Ding, *Front. Microbiol.*, 2018, **9**, 790.

26 J. Sawai, N. Ishizu and M. Itoh, *Biocontrol Sci.*, 2003, **8**, 123–127.
27 Y.-Y. Liao, A. L. Strayer-Scherer, J. White, A. Mukherjee, R. De La Torre-Roche, L. Ritchie, J. Colee, *et al.*, *Phytopathology*, 2019, **109**, 52–62.
28 Y. Liao, A. Strayer-Scherer, J. White, R. De La Torre-Roche, L. Ritchie, J. Colee, G. Vallad, J. Freeman, J. Jones and M. Paret, *Sci. Rep.*, 2019, **9**, 1–10.
29 Y.-Y. Liao, Y. Huang, R. Carvalho, M. Choudhary, S. Da Silva, J. Colee, A. Huerta, G. E. Vallad, J. H. Freeman and J. B. Jones, *Environ. Sci. Technol.*, 2021, **55**, 13561–13570.
30 Y. Y. Liao, J. Pereira, Z. Y. Huang, Q. R. Fan, S. Santra, J. C. White, R. de la Torre-roche, S. Da Silva, G. E. Vallad, J. H. Freeman, J. B. Jones and M. L. Paret, *Plants*, 2023, **12**(9), 1832.
31 M. Choudhary, Y.-Y. Liao, Z. Huang, J. Pereira, S. Santra, A. Parajuli, S. Da Silva, J. B. Jones, J. H. Freeman and M. L. Paret, *Plant Dis.*, 2023, 3234–3242.
32 J. R. Lamichhane, E. Osdaghi, F. Behlau, J. Köhl, J. B. Jones and J.-N. Aubertot, *Agron. Sustainable Dev.*, 2018, **38**, 28.
33 D. R. Hoagland and D. I. Arnon, *The water-culture method for growing plants without soil*, California Agricultural Experiment Station, 1938.
34 *Fact Sheet Reregistration Eligibility Decision (RED) Sulfur*, United States Environmental Protection Agency, 1991.
35 J. S. Williams and R. M. Cooper, *Plant Pathol.*, 2004, **53**, 263–279.
36 Z. L. Xu, P. C. Wang, H. B. Wang, Z. H. Yu, H. Y. Au-Yeung, T. Hirayama, H. Z. Sun and A. X. Yan, *J. Biol. Chem.*, 2019, **294**, 16978–16991.
37 D. Zhitnitsky, J. Rose and O. Lewinson, *Sci. Rep.*, 2017, **7**, 44554.
38 J. Pereira, A. King, M. G. Campos and S. Santra, *Curr. Nanosci.*, 2022, **18**, 410–424.
39 P. E. Russell, *J. Agric. Sci.*, 2005, **143**, 11–25.
40 Lime Sulfur Technical Report, P. R., Institute, United States Department of Agriculture, 2014.
41 R. Steudel, G. Holdt and R. Nagorka, *Z. Naturforsch., B:J. Chem. Sci.*, 1986, **41**, 1519–1522.
42 S. Licht and J. Davis, *J. Phys. Chem. B*, 1997, **101**, 2540–2545.
43 A. Kamyshny, A. Goifman, J. Gun, D. Rizkov and O. Lev, *Environ. Sci. Technol.*, 2004, **38**, 6633–6644.
44 R. Carvalho, K. Duman, J. B. Jones and M. L. Paret, *Sci. Rep.*, 2019, **9**, 20124.
45 P. Bellio, L. Fagnani, L. Nazzicone and G. Celenza, *MethodsX*, 2021, **8**, 101543.
46 J. Pereira, D. N. Moreno, G. G. Giannelli, E. Davidson, J. Rivera-Huertas, H. H. Wang and S. Santra, *Environ. Sci.: Nano*, 2023, **10**, 3012–3024.
47 E. Davidson, J. Pereira, G. G. Giannelli, Z. Murphy, V. Anagnostopoulos and S. Santra, *Molecules*, 2023, **28**, 6098.
48 D. Sharan, D. Wolfson, C. M. Green, P. Lemke, A. G. Gavin, R. J. Hamers, Z. V. Feng and E. E. Carlson, *Environ. Sci.: Nano*, 2023, **10**, 1978–1992.
49 A. Kamyshny, J. Gun, D. Rizkov, T. Voitsekovski and O. Lev, *Environ. Sci. Technol.*, 2007, **41**, 2395–2400.
50 G. Kresse and J. Hafner, *Phys. Rev. B:Condens. Matter Mater. Phys.*, 1993, **47**, 558–561.
51 G. Kresse and J. Hafner, *J. Phys.:Condens. Matter*, 1994, **6**, 8245–8257.
52 G. Kresse and J. Furthmuller, *Comput. Mater. Sci.*, 1996, **6**, 15–50.
53 G. Kresse and J. Furthmuller, *Phys. Rev. B:Condens. Matter Mater. Phys.*, 1996, **54**, 11169–11186.
54 G. Kresse and D. Joubert, *Phys. Rev. B:Condens. Matter Mater. Phys.*, 1999, **59**, 1758–1775.
55 J. P. Perdew, K. Burke and Y. Wang, *Phys. Rev. B:Condens. Matter Mater. Phys.*, 1996, **54**, 16533–16539.
56 K. Mathew, R. Sundararaman, K. Letchworth-Weaver, T. A. Arias and R. G. Hennig, *J. Chem. Phys.*, 2014, **140**, 8.
57 K. Mathew, V. S. C. Kolluru, S. Mula, S. N. Steinmann and R. G. Hennig, *J. Chem. Phys.*, 2019, **151**, 8.
58 S. B. Kedare and R. P. Singh, *J. Food Sci. Technol.*, 2011, **48**, 412–422.
59 S. L. Smith, M. G. Campos, A. Ozcan, H. C. Mendis, M. Young, M. E. Myers, M. Atilola, M. Doomra, Z. Thwin and E. G. Johnson, *J. Agric. Food Chem.*, 2021, **69**, 10807–10818.
60 M. Kah, D. Navarro, R. S. Kookana, J. K. Kirby, S. Santra, A. Ozcan and S. Kabiri, *Environ. Chem.*, 2019, **16**, 401–410.
61 S. A. Khan, R. W. Hughes and P. A. Reynolds, *Vib. Spectrosc.*, 2011, **56**, 241–244.
62 X. Chen, T. Hou, K. A. Persson and Q. Zhang, *Mater. Today*, 2019, **22**, 142–158.
63 F. E. Bedoya-Lora, A. Hankin and G. H. Kelsall, *Electrochim. Acta*, 2019, **314**, 40–48.
64 B. C. Smith, *Inorganics II: The Spectra*, 01 edn, 2024.
65 N. Thomas and M. Rajamathi, *Langmuir*, 2009, **25**, 2212–2216.
66 S. Choudhary, N. Oli, S. Shweta, S. Kumar, M. K. Bhattarai, C. A. Malca-Reyes, R. K. Katiyar, B. Tripathi, L. M. Díaz-Vázquez, G. Morell and R. S. Katiyar, *Molecules*, 2024, **29**, 5116.
67 H. W. Chen, C. H. Wang, W. L. Dong, W. Lu, Z. L. Du and L. W. Chen, *Nano Lett.*, 2015, **15**, 798–802.
68 C. R. Matos, M. J. Xavier, L. S. Barreto, N. B. Costa and I. F. Gimenez, *Anal. Chem.*, 2007, **79**, 2091–2095.
69 M. El Bouraie and A. A. Masoud, *Appl. Clay Sci.*, 2017, **140**, 157–164.
70 K. Tsuchiya, S. Fuchida and C. Tokoro, *J. Environ. Chem. Eng.*, 2020, **8**, 104514.
71 A. Ryzhikov, V. Hulea, D. Tichit, C. Leroi, D. Anglerot, B. Coq and P. Trens, *Appl. Catal., A*, 2011, **397**, 218–224.
72 A. T. Vu, S. Jiang, Y. H. Kim and C. H. Lee, *Ind. Eng. Chem. Res.*, 2014, **53**, 13228–13235.
73 D. Y. Zhang, P. X. Zhang, S. H. Song, Q. H. Yuan, P. Yang and X. Z. Ren, *J. Alloys Compd.*, 2014, **612**, 315–322.
74 M. T. Dang, N. T. Long, V. B. T. Phung, N. T. B. Trang, T. A. Nguyen, T. N. Tran, N. V. A. Duy, N. T. Van, N. V. Nghia and P. Schall, *Appl. Surf. Sci.*, 2025, **687**, 162210.

75 M. Rana, S. A. Ahad, M. Li, B. Luo, L. Z. Wang, I. Gentle and R. Knibbe, *Energy Storage Mater.*, 2019, **18**, 289–310.
76 Z. Xu, Z. Qiu, Q. Liu, Y. Huang, D. Li, X. Shen, K. Fan, J. Xi, Y. Gu and Y. Tang, *Nat. Commun.*, 2018, **9**, 3713.
77 M. Young and S. Santra, *J. Agric. Food Chem.*, 2014, **62**, 6043–6052.
78 A. Strayer-Scherer, Y. Y. Liao, M. Young, L. Ritchie, G. E. Vallad, S. Santra, J. H. Freeman, D. Clark, J. B. Jones and M. L. Paret, *Phytopathology*, 2018, **108**, 196–205.
79 Q. Fan, Y.-Y. Liao, S. Kunwar, S. Da Silva, M. Young, S. Santra, G. V. Minsavage, J. H. Freeman, J. B. Jones and M. L. Paret, *Crop Prot.*, 2021, **139**, 105366.
80 M. Zhu, Y. Li, X. S. Long, C. Y. Wang, G. P. Ouyang and Z. C. Wang, *Int. J. Mol. Sci.*, 2022, **23**, 11947.
81 M. Zhu, Y. Li, D. P. Chen, C. P. Li, G. P. Ouyang and Z. C. Wang, *Pest Manage. Sci.*, 2023, **79**, 537–547.
82 R. A. Dop, D. R. Neill and T. Hasell, *ACS Appl. Mater. Interfaces*, 2023, **15**, 20822–20832.
83 K. S. Cho, M. Hirai and M. Shoda, *Appl. Environ. Microbiol.*, 1992, **58**, 1183–1189.
84 M. A. Gatou, E. Skylla, P. Dourou, N. Pippa, M. Gazouli, N. Lagopati and E. A. Pavlatou, *Crystals*, 2024, **14**, 215.
85 Y. H. Leung, A. M. Ng, X. Xu, Z. Shen, L. A. Gethings, M. T. Wong, C. M. Chan, M. Y. Guo, Y. H. Ng and A. B. Djurišić, *Small*, 2014, **10**, 1171–1183.
86 Y. He, S. Ingudam, S. Reed, A. Gehring, T. P. Strobaugh and P. Irwin, *J. Nanobiotechnol.*, 2016, **14**, 1–9.
87 Y. Nakamura, K. Okita, D. Kudo, D. N. D. Phuong, Y. Iwamoto, Y. Yoshioka, W. Ariyoshi and R. Yamasaki, *Nanomaterials*, 2021, **11**, DOI: 10.3390/nano11061584.
88 A. Aroca, C. Gotor and L. C. Romero, *Front. Microbiol.*, 2018, **9**, 1369.
89 L. O. Fuentes-Lara, J. Medrano-Macías, F. Pérez-Labrada, E. N. Rivas-Martínez, E. L. García-Enciso, S. González-Morales, A. Juárez-Maldonado, F. Rincón-Sánchez and A. Benavides-Mendoza, *Molecules*, 2019, **24**.
90 B. Dutta, R. Gitaitis, S. Smith and D. Langston, *PLoS One*, 2014, **9**, e99215.
91 T. Nishioka, Y. Takai, T. Mishima, M. Kawaradani, H. Tanimoto, K. Okada, T. Misawa and S. Kusakari, *Biocontrol Sci.*, 2016, **21**, 37–43.
92 L. D. Marchioretto, A. De Rossi, L. O. do Amaral and A. Ribeiro, *Sci. Hortic.*, 2019, **246**, 634–642.
93 W. C. Allen, T. Kon and S. M. Sherif, *Horticulturae*, 2021, **7**, 308.
94 Y. Y. Li, Y. Liu, C. J. Wu, R. Zhao, M. H. Li, J. Cai, L. Ma, X. K. He, X. M. Wu and Z. Zhenhua, *Front. Plant Sci.*, 2023, **14**, 1257672.
95 P. F. Zhang, Y. Y. Dai, S. Masateru, M. Natsumi and I. Kengo, *Commun. Soil Sci. Plant Anal.*, 2017, **48**, 2601–2611.
96 R. M. Pacheco, R. Verón and S. Cáceres, *Rev. Fac. Cienc. Agrar.*, 2019, **51**, 19–28.
97 S. H. Zhang, Z. P. Bao, Y. L. Wu, Y. Wang, R. Liu, Y. X. Gao, X. D. Zhao, C. H. Zhang and F. P. Du, *ACS Sustainable Chem. Eng.*, 2023, **11**, 15385–15396.
98 A. K. Johnson, F. W. Roeth, A. R. Martin and R. N. Klein, *Weed Technol.*, 2006, **20**, 893–897.
99 G. Doruchowski, W. Swiechowski, S. Masny, A. Maciesiak, M. Tartanus, H. Bryk and R. Holownicki, *Sci. Total Environ.*, 2017, **575**, 1239–1246.
100 K. W. Park and E. M. Leitao, *Chem. Commun.*, 2021, **57**, 3190–3202.
101 S. M. Kim, S. Roy, K. S. Yoon and J. W. Rhim, *Packag. Technol. Sci.*, 2021, **34**, 505–516.
102 I. A. Massalimov, A. E. Chuikin, B. I. Massalimov and A. G. Mustafin, *Nanotechnologies in Construction*, 2023, **15**, 27–36.
103 M. Hawkesford, W. Horst, T. Kichey, H. Lambers, J. Schjoerring, I. S. Moller and P. White, *Functions of Macronutrients*, 3rd edn, 2012.
104 M. Lu, D. Y. Liu, Z. M. Shi, X. P. Gao, Y. Liang, Z. Yao, W. Zhang, X. Z. Wang and X. P. Chen, *J. Sci. Food Agric.*, 2021, **101**, 582–592.
105 Z. Wang, M. Ul Hassan, F. Nadeem, L. Q. Wu, F. S. Zhang and X. X. Li, *Front. Microbiol.*, 2020, **10**, 495191.
106 B. M. Santos, C. E. Esmel, J. E. Rechcigl and H. Moratinos, Effects of sulfur fertilization on tomato production, in *Proceedings of the Florida State Horticultural Society*, 2007, vol. 120, pp. 189–191.
107 C. E. Esmel, B. M. Santos, E. H. Simonne, J. E. Rechcigl and J. W. Noling, *HortTechnology*, 2012, **22**, 523–527.
108 Z. Tietel, U. Yermiyahu and A. Bar-Tal, *Agronomy*, 2022, **12**, 1117.
109 I. A. Massalimov, A. R. Shainurova, A. N. Khusainov and A. G. Mustafin, *Russ. J. Appl. Chem.*, 2012, **85**, 1832–1837.
110 K. J. Rao and S. Paria, *RSC Adv.*, 2013, **3**, 10471–10478.
111 S. Shankar and J. W. Rhim, *Food Hydrocolloids*, 2018, **82**, 116–123.
112 X. S. Cao, C. A. X. Wang, X. Luo, L. Yue, J. C. White, W. Elmer, O. P. Dhankher, Z. Y. Wang and B. S. Xing, *ACS Nano*, 2021, **15**, 11817–11827.
113 X. S. Cao, Y. L. Liu, X. Luo, C. X. Wang, L. Yue, W. Elmer, O. P. Dhankher, J. C. White, Z. Y. Wang and B. S. Xing, *Sci. Total Environ.*, 2023, **884**, 11817–11827.
114 Y. Wang, C. Y. Deng, W. H. Elmer, C. O. Dimkpa, S. Sharma, G. Navarro, Z. Y. Wang, J. LaReau, B. T. Steven, Z. Y. Wang, L. J. Zhao, C. Q. Li, O. P. Dhankher, J. L. Gardea-Torresdey, B. S. Xing and J. C. White, *ACS Nano*, 2022, **16**, 11204–11217.
115 K. Imada, S. Sakai, H. Kajihara, S. Tanaka and S. Ito, *Plant Pathol.*, 2016, **65**, 551–560.